Optimization of Body Pressure Relief Support Wearable Devices Integrating 3D Printing and Gait Recognition Algorithms

Yaqiong Zhou*, Bing Hu
School of Fine Arts and Design, Hefei Normal University, Hefei, 230601, China

***Abstract*—To improve wearing comfort and achieve individual recognition, this study designs an ankle exoskeleton that simulates natural human movement based on the joint structure of the human lower limbs. The function of the sole spring is achieved through compression springs on the exoskeleton framework coupled with the foot, and a customized insole is designed using 3D printing technology. This study uses a gait recognition algorithm based on a convolutional gated recurrent unit fully convolutional network with a dual attention mechanism to achieve individual recognition. The results showed that compared to the natural state, when walking with exoskeletons, the integrated electromyographic signals of the gastrocnemius and tibialis anterior muscles decreased by 5.4% and 3.6%, respectively, and the intelligent insole reduced plantar pressure to a certain extent. The accuracy of the proposed gait recognition algorithm could reach 95.26%, which was 2.03% higher than that of fully convolutional networks. In addition, the fuzzy output signals of the left and right feet were combined to obtain the proportions of single support phase and double support phase during walking, which were 92.7% and 7.3%, respectively. This study indicates that a body pressure reducing support wearable device that integrates 3D printing and gait recognition algorithms can reduce lower limb joint pressure, providing a new possibility for improving wearing comfort and achieving individual recognition. It also helps to improve the quality of life for the target audience.**

***Keywords*—3D printing; gait recognition; body decompression support; wearing devices; electromyographic signal**

I. Introduction

A. Research Background

With the intensification of the aging trend in society, the demand for Body Pressure Relief Support Wearable Devices (BPRSWDs) is increasing in the elderly and rehabilitation medicine fields. This type of device aims to provide personalized support and soothing effects through real-time monitoring and analysis of the wearer's body, in order to improve their quality of life [1]. However, the current BPRSWDs still need to be improved in terms of functionality and performance. In recent years, Gait Recognition (GR) technology, as an emerging biometric recognition method, has been widely applied in the field of security due to its advantages of non-contact and long-distance monitoring [2]. This technology can effectively distinguish gait features between different individuals by analyzing gait images. However, the current application of GR methods in BPRSWDs is not yet sufficient [3]. In addition, the development of Three-dimensional Printing Technology (3D-PT) has provided the possibility for customized and personalized design of BPRSWDs [4-5]. However, previous studies have not fully considered the impact of human lower limb joint structure on wearing comfort, and there is a lack of effective GR algorithms to achieve individual recognition.

B. Research Method and Objectives

In order to improve wearing comfort and achieve individual recognition, this study proposes a BPRSWDs optimization method that integrates 3D-PT and GR algorithm. Firstly, the design combines customized body support components with 3D-PT, and then utilizes GR technology to monitor and analyze the wearer's gait characteristics in real-time. The contribution of the research is the design of a body pressure reducing support wearable device based on 3D printing technology, as well as the proposal of a gait recognition algorithm based on a convolutional gated recurrent unit full convolutional network with dual attention mechanism, which achieves individual identity recognition. This device provides new design ideas and methods for the field of body stress relief support wearable devices by improving wearing comfort and algorithm accuracy. It is expected to provide a more comfortable and personalized experience for the audience, thereby improving the quality of life.

C. Organization Structure

The research content consists of five sections. Section I is a summary of research related to 3D printing, wearable devices, and GR. Related works is given in Section II. Section III is the design of BPRSWDs and GR algorithms, and application analysis is conducted in Section IV. Section V summarizes the entire study.

II. Related Works

3D printing is a technology that uses digital model files as the basis and adhesive materials such as powdered metal or plastic to construct objects through layer by layer printing. Peki et al. used glass fiber reinforced UV cured polymer matrix composites for robot 3D printing and optimized parameters such as nozzle diameter. Under specific parameter conditions, 3D printing could achieve high tensile and bending strength [6]. Yu's team proposed a novel high current planar inductor with heat dissipation fins based on 3D printing, and conducted experiments using selective laser melting technology to 3D print copper windings. At a current of 100A, this inductor could function well, while traditional inductors could not function due to high temperatures [7]. Wu's team has prepared a 3D printed

conductive polymer ink with high conductivity, flexible stretchability, and strain sensing monitoring performance. Silane modified conductive polymers have excellent printability and strain sensing properties [8]. Zhang et al. proposed the latest progress of 3D printing in the field of wearable electrochemical energy devices and explored its applications and limitations in this field. Although 3D-PT has great potential in wearable energy devices, issues such as ink formulation and material design still needed to be addressed [9]. Liu's team explored the manufacturing of Flexible Strain Sensors (FSS) through 3D-PT and conducted in-depth discussions on the sensing mechanism of 3D-printed FSSs. 3D-PT had great potential in manufacturing FSSs and could bring revolutionary changes to the development of wearable devices and electronic skins [10]. Hong et al. designed a capacitive pressure sensor using a biomimetic cheetah leg microstructure, optimized the structural parameters using 3D-PT, and achieved high sensitivity, wide pressure range, fast response time, and excellent durability [11].

GR is a technology that identifies human movements such as walking and running by analyzing the characteristics of human motion trajectory, dynamics, and physiological signals. Bianco's team proposed a GR system based on inertial sensors, which recognizes gestures, user gait, and identity through custom wristbands and recursive neural network-based algorithms. The recognition accuracy and user satisfaction of the system could reach 90% [12]. Lee et al. employed a method based on Inertial Measurement Unit (IMU) and Long Short Term Memory (LSTM) machine learning models to identify gait under different fatigue states. The LSTM model had the highest accuracy in identifying simulated gait, with the combination of toe and sacral IMU achieving the highest accuracy of 95.71% [13]. Semwal et al. used a hybrid deep learning model, combined with data collected by IMU sensors, to achieve recognition of various gait activities. The proposed hybrid framework based on ensemble learning performed excellently in GR, with an accuracy rate of 99.34% [14]. Ma's research team has proposed a high-performance GR and efficient energy harvesting method. It filtered the impact of energy storage on the electrical signal of the piezoelectric energy harvester through preprocessing algorithms, and used a classifier based on LSTM network to accurately capture time information in gait induced power generation. Compared to state-of-the-art architectures, this method has improved gait recall by 12%, achieved energy harvesting efficiency of up to 127%, and reduced power consumption by 38% [15]. Hasan's team proposed a new stacked auto-encoder method to address the impact of perspective changes on human GR in a multi camera environment. By learning discriminative perspective invariant gait representation, this method could gradually convert bone joint coordinates from any view to a common normative view while preserving temporal information. The average correct class recognition of this method could reach 33.86% [16].

In summary, many researchers have made different designs for 3D-PT and GR. However, these studies mainly focus on the optimization of materials and processes, with less attention paid to performance evaluation and optimization in different application scenarios. At the same time, the universality and practicality of GR technology still need to be improved, and the accuracy in practical applications still needs to be improved. Therefore, this study integrates 3D-PT and GR algorithms to conduct optimization research on BPRSWDs, with the aim of providing users with a more comfortable wearing experience.

III. Optimization Design of BPRSWDs Integrating 3D-PT and GR Algorithm

This section mainly designs the GR algorithm based on Convolutional Bi-directional Gated Recurrent Unit Fully Convolutional Networks (ConvBiGru-FCN). This algorithm extracts discriminative features by analyzing the walking patterns of the human body, achieving recognition of individual identity.

A. The Overall Design of BPRSWDs

The design of BPRSWDs is based on the structure of human lower limb joints, simulating natural human movement, aiming to reduce joint pressure and improve comfort [17].

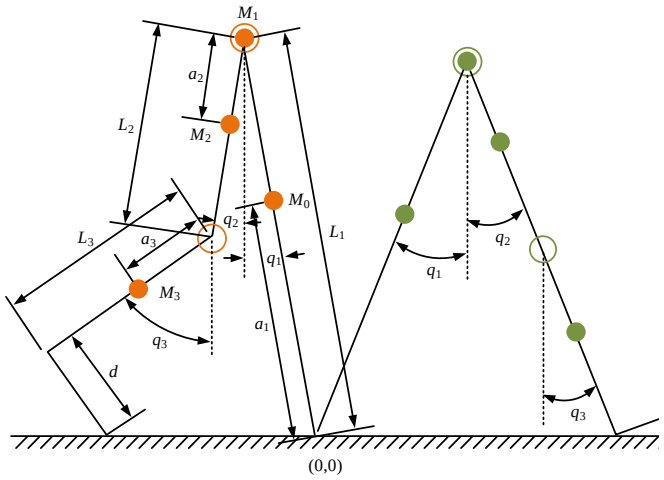

Fig. 1. A human walking model within a single support phase.

In Fig. 1, the unilateral lower limb movement state during human walking is divided into support phase and swing phase. The Single Support Phase (SSP) model of a single leg simplifies the support leg, support phase foot, swing phase thigh, swing phase calf, and swing phase foot into members [18]. The model contains three degrees of freedom, namely the hip joint of the supporting leg, the hip joint of the swinging leg, and the knee joint of the swinging leg. The angle between the rod and the vertical axis of the human body is q_i, the length of the rod is L_i, the distance between the center of mass of the rod and the lower limb joint is a_i, and the moment of inertia of the rod is I_i, $i=1,2,3$. The foot length is d, and the supporting ankle joint is the coordinate origin. The centroid coordinates of the supporting leg, upper body, swinging thigh, and swinging calf are $M_0(x_0,y_0)$, $M_0(x_1,y_1)$, $M_0(x_2,y_2)$, and $M_0(x_3,y_3)$, respectively. Introducing plantar springs in walking models can reduce human energy loss [19]. Based on this principle, an ankle exoskeleton is designed, which simulates the function of plantar springs through compression springs on the exoskeleton framework coupled with the human foot.

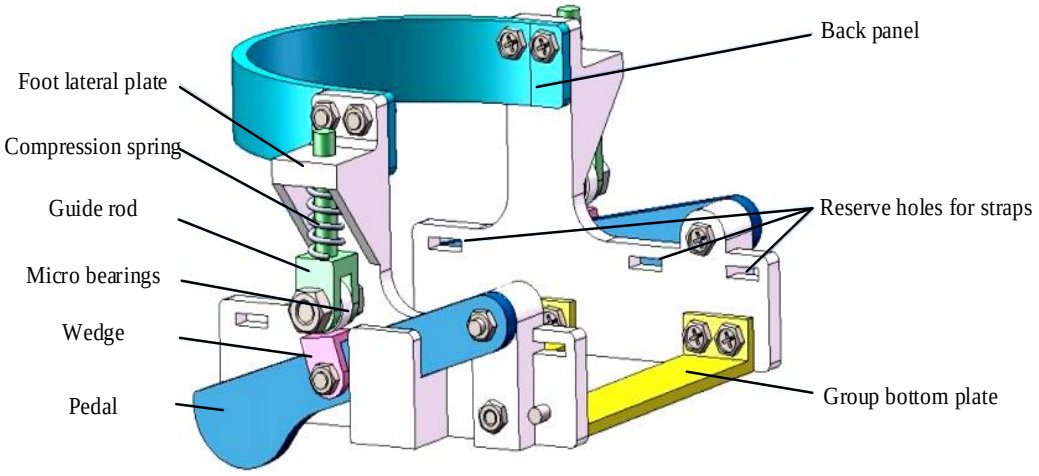

Fig. 2. The overall structure of ankle exoskeleton.

As shown in Fig. 2, the exoskeleton is mainly composed of multiple components, such as the foot side plate, compression spring, guide rod, micro bearings, wedges, pedals, backplate, and plantar plate. These components are fixed together through connectors. The shoes worn by the experimenter are tightly attached to the main frame composed of the foot side panel, back panel, and sole panel, and are fixed to the front of the shoes with straps. The sole plate is responsible for supporting the weight of the human body, and aluminium alloy materials with high strength and good wear resistance are selected. The pedal is made of carbon fiber board and forms a rotating pair connection with the foot side panel, with the rotation center located in the middle of the foot. There is a vertical plane on the foot side plate that bears elastic force, and the strengthening ribs on both sides increase the strength of the force bearing surface [20-21]. The concave platform below the foot side panel can limit the pedal and prevent it from bending outward. The other components are made by UV curing printing, using lightweight and moderately rigid photosensitive resin materials. The ankle exoskeleton is located in the middle and rear of the foot and does not affect the force exerted by the human toes when they are off the ground. The passive energy storage structure is a crucial part of the ankle exoskeleton, which can collect energy from the foot following the ground and release it when the heel leaves the ground. This structure mainly includes pedals, guide rods, compression springs, and wedges. During walking, when the vertical distance between the end of the pedal and the ground is less than 10mm, the pedal will rotate, driving the compression spring of the guide rod [22-23]. During the mid support phase, the sole of the foot is completely in contact with the ground, and the elastic force is in the vertical direction, assisting in ankle dorsiflexion movement. When the heel leaves the ground, the elastic potential energy is released, and the spring pushes the foot side plate to rotate. In addition, the selection and parameter design of compression springs give them appropriate stiffness and compression stroke. The assembled ankle exoskeleton has a mass of 235g and does not affect normal foot movement. It can feel the pulse force when the heel is off the ground during walking. The stiffness calculation of the unilateral spring is Eq. (1).

$$k = \frac{Gw^4}{8nD^3} \tag{1}$$

In Eq. (1), the stiffness of the unilateral spring is k, and the shear modulus of elasticity is G. The diameter of the compression spring is w, the center diameter is D, and the effective number of turns is n. The shape and material stiffness of customized insoles have a significant impact on plantar pressure. Choosing materials with lower stiffness can increase the contact area between the foot and insole, and reduce plantar pressure. After damage to the plantar fascia, the height of the arch of the foot decreases, increasing the tension of the plantar ligaments and the stress on the midfoot and metatarsal bones. To prevent foot arch lodging and enhance arch stiffness, a support structure that fits the arch of the foot has been added to the flat insole. Through 3D-PT, different stiffness-filling patterns and unique insole shapes can be designed to meet the needs of different wearers. This study divides insoles into buffer zones and fit zones. The buffer zone includes the forefoot and heel, while the fit zone includes the middle of the foot. The buffer zone adopts a porous negative Poisson's ratio structure, which has a lightweight buffering effect. The fitting area is composed of an Arch Support Structure (ASS) and a honeycomb structure, which increases the contact surface between the ASS and the sole of the foot. The honeycomb structure is lightweight and has high stiffness. Finally, the Thermoplastic Polyurethanes (TPU) is selected as the insole material, which has good elasticity and wear resistance, meeting the comfort and safety requirements of medical insoles.

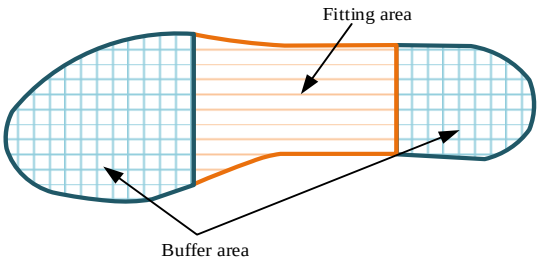

Fig. 3. Insole area division.

In Fig. 3, the design of the insole buffer zone is mainly aimed at the forefoot and heel, using a porous negative Poisson's ratio structure to increase contact area and reduce internal stress. This structure has special mechanical properties, which can cause lateral expansion when subjected to uniaxial longitudinal tension and lateral contraction when compressed, thereby improving buffering performance. Negative Poisson's ratio structures can be divided into two types: concave and porous, where concave structures generate two-dimensional rotation when subjected to tension. Porous structures achieve negative Poisson's ratio effects through the elastic instability of the material [24-25]. The structural design of the fitting area of the insole mainly adopts honeycomb structure and ASS. Honeycomb structure is a porous biomimetic structure with high strength and high stiffness ratio, which can effectively improve the support capacity of the bonding area. ASS helps to reduce shock absorption and disperse the weight transmitted to the sole of the foot, reducing excessive tension between the arch ligaments and muscles. In the design process, 3D scanning technology is first used to capture a realistic foot model of the human body, and then ASS is obtained through Boolean operations. Finally, ASS and honeycomb structure form the insole bonding area [26].

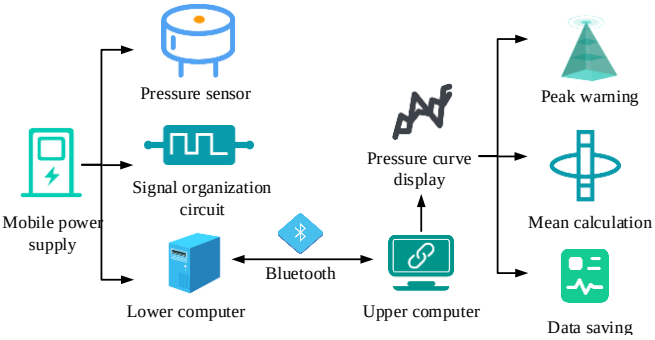

Fig. 4. Design of insole collection system.

In the insole collection system shown in Fig. 4, eight thin film sensors are distributed on the medical insole to collect pressure information. These sensors convert analog signals into digital signals through their built-in analog-to-digital converters. The wireless transmission module transmits digital signals to the upper computer powered by a 12V mobile power supply. The upper computer calculates the pressure value based on the load voltage fitting curve of sensors at different positions, and records the pressure peak, displays the plantar pressure curve, and saves data on the computer end. The output of the signal conditioning circuit is Eq. (2).

$$V_{out} = \frac{R}{R_s} V_{ref} = \frac{F}{K_c} R V_{ref} \tag{2}$$

In Eq. (2), the output of the signal conditioning circuit is V_{out}. The reference voltage is V_{ref}. The reference resistance is R. The resistance value of the pressure sensor under positive pressure F is R_s. The sensor coefficient is K_c.

B. Design of GR Algorithm

The main purpose of the GR algorithm is to extract discriminative features by analyzing the walking patterns of the human body to achieve individual identity recognition. Its key technologies include Gait Feature Extraction (GFE) and feature similarity calculation [27]. During the registration phase, users wear BPRSWDs while walking, and sensors collect data and upload it to the server. The server uses a Feature Extraction Network (FEN) to extract walking gait features and analyze the body's stress relief support. In the authentication stage, the server extracts the current walking features and calculates the similarity with the registration template [28].

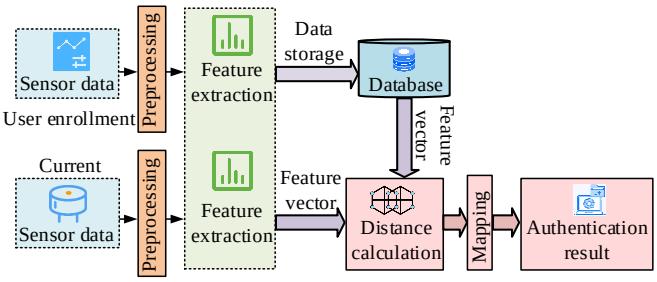

Fig. 5. Identity recognition system based on GR.

In Fig. 5, FEN is the core of the identity recognition system, responsible for extracting unique walking features from the swinging acceleration and angular velocity time series [29]. The characteristic of Full Convolutional Networks (FCN) based on time series features is that it does not include local pooling layers during the convolution process and maintains the length of the time series unchanged [30]. On this basis, this study proposes ConvBiGru-FCN for GFE. Convolutional Neural Network (CNN) is based on convolutional computation and constructs features by integrating spatial and channel information between levels. Previous studies have mainly focused on improving the quality of spatial coding and enhancing feature expression capabilities [31]. The Squeeze Excitation (SE) module focuses on the interdependence between channels and adaptively calibrates channel characteristic responses. This study improves the SE module to make it suitable for time-series feature extraction and implements a one-dimensional channel attention mechanism to distinguish the focus points and channel feature contributions of different convolutional kernels, thereby improving the effectiveness of gait identity recognition. The compression calculation in the SE module is Eq. (3).

$$z_c = F_{sq}(u_c) = \frac{1}{T}\sum_{i=1}^{T} u_c(i) \tag{3}$$

In Eq. (3), the compressed value of the channel is z_c, the compression operation is F_{sq}, the input feature map is u_c, and the time length is T. The calculation of incentive operation is Eq. (4).

$$s = F_{ex}(z, W) = \sigma(W_2 \delta(W_1 z)) \tag{4}$$

In Eq. (4), the channel weight vector is s and the excitation operation is F_{ex}. The vector obtained from the previous layer is z. The weight information obtained through learning is W. The parameter matrices are W_1 and W_2,

respectively. The Sigmoid and Relu activation functions are σ and δ. The weight update calculation is Eq. (5).

$$\tilde{x}_c = F_{scale}(u_c, s_c) = s_c u_c \tag{5}$$

In Eq. (5), the feature map obtained by updating the feature map with the weight vector is $\tilde{x}_c$, and the update operation is F_{scale}. By introducing the SE module, weight coefficients are assigned to each channel feature to achieve a channel based attention mechanism. This makes the model focus more on features that contribute significantly to GR, suppresses channel features that contribute less or no, and improves the model's identification ability for each channel feature. Another attention mechanism obtains weight vectors and updates feature map weights through the Dense layer and Softmax function. The ConvBiGru-FCN network obtained by combining the above two attention mechanisms is Fig. 6.

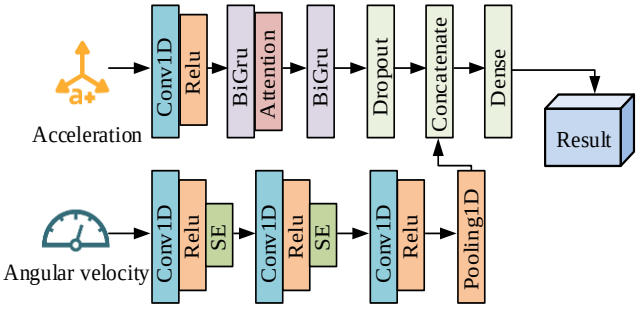

Fig. 6. Structure of ConvBiGru-FCN networks.

ConvBiGru-FCN uses FCN and Bidirectional Gated Recurrent Unit (BiGru) to extract feature information in parallel. FCN consists of three convolutional blocks and excels in time series classification. The BiGru module enhances the feature extraction ability of FCN, with a simpler structure, fewer parameters, and easier training convergence. To match the input dimension, a one-dimensional convolutional layer is added before BiGru instead of a permutation layer, as it has a certain degree of time series noise suppression ability, which helps to improve the feature extraction ability of the model. ConvBiGru-FCN introduces attention mechanism on the basis of the original structure to improve feature extraction ability. To add Attention Mechanism 1 in the FCN section, focusing on important features. To add Attention Mechanism 2 to the BiGru section to enhance the ability to capture bidirectional time series information. After dual channel feature extraction and feature layer fusion, the network outputs gait features through a fully connected layer. One of the key technologies of GR is to calculate the similarity between the current user's walking characteristics and the user feature template. The calculation process of the feature vector template is Eq. (6).

$$T_i = \frac{1}{n}\sum_{j=1}^{n} F(s_{ij}) \tag{6}$$

In Eq. (6), the feature vector template of the i-th user is T_i. The GFE network is F. The j-th walking sequence of user i during the registration process is s_{ij}. The number of time series in the registration phase is n. The calculation of gait similarity is Eq. (7).

$$d(x, y) = \frac{x \cdot y}{|x|^2 + |y|^2 - x \cdot y} \tag{7}$$

In Eq. (7), the eigenvectors of two time series are x and y respectively, and the distance between the two is $d(x, y)$. The normalization function converts distance values into similarity probabilities, and the calculation process is Eq. (8).

$$P = F_N(d(x, y)) \tag{8}$$

In Eq. (8), the similarity probability is P and the normalization function is F_N. To improve the generalization ability of GFE network and improve the accuracy of identity recognition system, this study uses Time-series Generative Adversarial Network (TimeGAN) to enhance the gait temporal dataset to solve the problem of small data volume and insufficient samples in practical scenarios. The TimeGAN structure is Fig. 7.

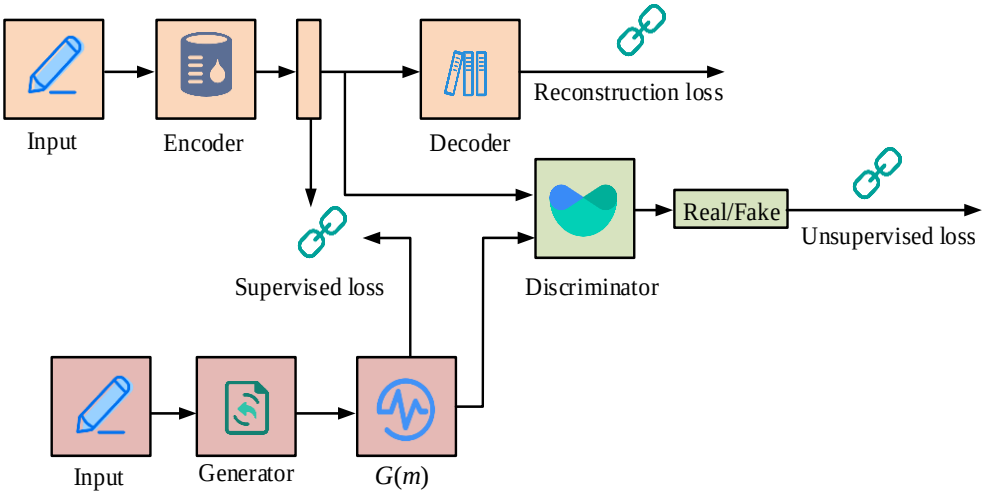

Fig. 7. TimeGAN structure.

TimeGAN is a temporal data generation enhancement method that combines unsupervised GAN and supervised auto-regressive models. It mainly consists of embedding function, recovery function, sequence generator, and sequence discriminator. The characteristic of TimeGAN is the joint training of automatic encoding components (embedding function and recovery function) and adversarial components (sequence generator and sequence discriminator), enabling it to simultaneously learn encoding features, generate sequence representations, and iterate across time, thereby maintaining temporal dynamic characteristics. The TimeGAN reconstruction loss function is Eq. (9).

$$L_R = MSE(G(m), m) \tag{9}$$

In Eq. (9), the reconstruction loss function is L_R, and the original input timing data is m. The timing data generated by the generator is $G(m)$, and the mean square error is calculated as MSE. The unsupervised loss calculation is Eq. (10).

$$L_U = -\alpha \cdot \sum_{i=1}^{n} (G(m[q]) * G(m[q+1])) \tag{10}$$

In Eq. (10), the unsupervised loss function is L_U, the regularization function is α, and a certain position in the sequence is q. The calculation of the supervised loss function is Eq. (11).

$$L_S = -\sum [r * \log(p(r \mid g(m)))] \tag{11}$$

In Eq. (11), the supervised loss function is L_S, and the true label is r. The probability distribution corresponding to the time series data generated by the generator is $p(r \mid g(m))$. The optimization function of TimeGAN is Eq. (12).

$$\min_{\theta_e, \theta_r} (\lambda L_S + L_R) \tag{12}$$

In Eq. (12), the embedded and restored network parameters are θ_e and θ_r, respectively, and the coefficient of the supervised loss function is λ. The second optimization function of TimeGAN is Eq. (13).

$$\min_{\theta_g} (\eta L_S + \max_{\theta_d} L_U) \tag{13}$$

In Eq. (13), the network parameters of the generator and discriminator are θ_g and θ_d, respectively, and the coefficient of the supervised loss function is η. This study uses TimeGAN to generate gait time series data to supplement the existing collected gait dataset and verify the effectiveness of identity GR. During the GR process, the pressure signals of the four sensors are F_1, F_2, F_3, and F_4. The proportion calculation of pressure information is Eq. (14).

$$\begin{cases} F_A = \dfrac{F_1}{F_1 + F_2 + F_3 + F_4 + N} \\ F_B = \dfrac{F_2}{F_1 + F_2 + F_3 + F_4 + N} \\ F_C = F_3 + \dfrac{F_4}{F_1 + F_2 + F_3 + F_4 + N} \\ F_N = \dfrac{N}{F_1 + F_2 + F_3 + F_4 + N} \end{cases} \tag{14}$$

In Eq. (14), the proportion of pressure at the heel, arch, and sole in the total is F_A, F_B, and F_C. The constant parameter is N. The proportion of a constant in the total is F_N. Before dealing with fuzzification, it is necessary to determine the fuzzy membership function and rule table. Fuzzy sets include two states: Positive Big (PB) and Zero Small (ZS). When the pressure ratio value is greater than the threshold, the fuzzy set is PB, and vice versa, it is ZS. Based on this, the fuzzy rule setting includes four states: early support, middle support, late support, and swing phase.

IV. Results and Discussion

The experiment uses 3D-PT to manufacture insoles with pressure reducing effects. By comparing the Electromyographic Signals (EMGS) of natural walking and wearing exoskeleton walking, the pressure reducing effect of intelligent insoles is verified. The GR algorithm is trained using ConvBiGru-FCN and compared with other networks in terms of performance.

A. Manufacturing and Forming of BPRSWDs

The experiment uses a Makerpi K5 Plus 3D printer to print BPRSWDs insoles. The printing process is divided into two parts: front and back. The front and rear parts of the insole are connected by two wedge-shaped blocks. The experiment explores 3D printing parameters, and Table I shows the final optimized parameters.

TABLE I. 3D Printing Parameters

Serial number	Parameter	Numerical value	Unit
1	Layer thickness	0.2	mm
2	Fill rate	20	%
3	Printing speed	40	mm/s
4	Nozzle temperature	210	℃
5	Hot bed temperature	75	℃
6	Consumable diameter	1.75	mm

After the 3D printing parameters are set, they are imported into the Cura printing processing software. After printing, glue is used to stick the front and rear parts, and waiting for the glue to settle and solidify before use. The 3D printer and physical image are shown in Fig. 8.

(a) Makerpi K5 Plus 3D printer (b) Physical image of insole

Fig. 8. 3D printers and physical images.

To collect plantar pressure from the human body, a Flexiforce A201 thin film pressure sensor is used in the experiment and installed on the surface of the insole. Four force measurement areas have been set on the insole, located at the first metatarsal bone, the third metatarsal bone, the arch of the foot, and the heel bone. Among them, sensors 1, 2, and 4 are used to reflect areas with high stress on the soles of the feet, and the magnitude of the pressure peak reflects the health of the feet. Sensor 3 is located on the arch fitting structure of the foot to verify its ability to withstand human weight. The experiment uses a dual track treadmill platform to provide different walking speeds and ground slopes for people wearing exoskeletons indoors. The experimental environment mainly includes a treadmill, muscle electrodes, sensor system, and upper computer. In the experiment, researchers compares the EMGS of natural walking and wearing exoskeletons to evaluate the decompression support effect of ankle exoskeletons. The EMGS of natural walking and walking with exoskeletons after bandpass filtering are displayed in Fig. 9.

Fig. 9(a) shows the EMGS during natural walking. The plantar and dorsiflexion movements of the foot involve the muscles on the anterior and posterior sides of the calf, and the EMGS fluctuate violently after being flat, with a significant phase difference between the two signals. Fig. 9(b) shows the EMGS of walking with an exoskeleton. Changes in the characteristics of EMGS can help muscles enhance strength and reduce fatigue, but may affect natural contraction and relaxation. The integrated value of EMGS is Fig. 10.

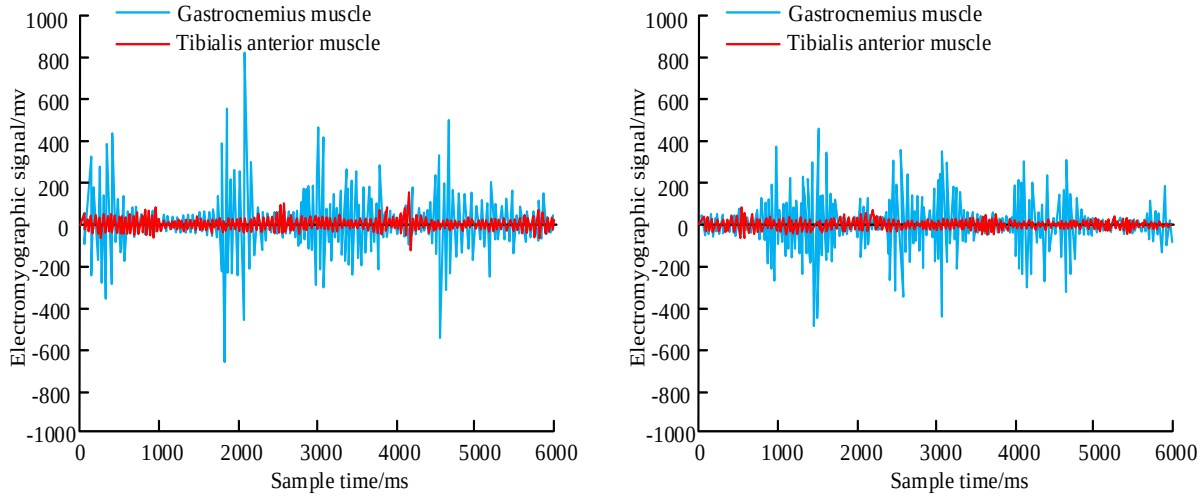

Fig. 9. The EMGS of human natural walking and walking with exoskeletons after bandpass filtering.

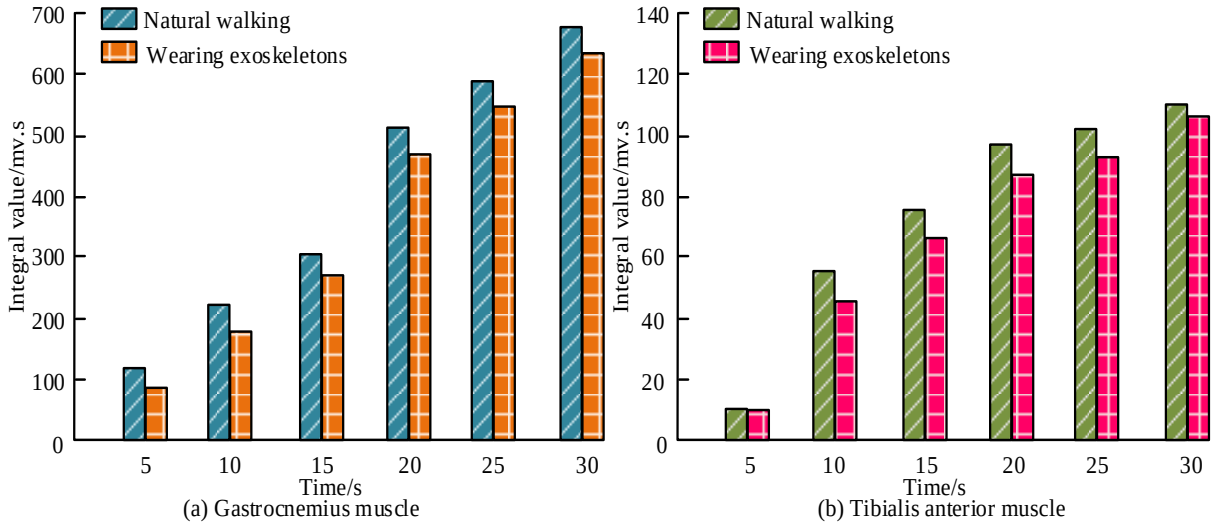

Fig. 10. Integrated value of EMGS.

Fig. 10(a) and 10(b) show the integrated values of gastrocnemius EMGS and anterior tibial EMGS for natural walking and walking with exoskeletons. When the human body wears exoskeletons, the EMGS integral values of the gastrocnemius and tibialis anterior muscles in the lower leg decrease. Compared to the natural state, when walking with exoskeletons, the EMGS integral values of the gastrocnemius and tibialis anterior muscles decreases by 5.4% and 3.6%, respectively. This indicates that the contraction characteristics of the lower limb muscles have been weakened, thereby proving that the ankle exoskeleton has a certain assisting effect. To verify the pressure reducing effect of intelligent insoles, a static plantar pressure measurement experiment is designed. The experiment uses a laser cutting machine to make acrylic boards of the same size as insoles, and divides them into eight areas. Volunteers stand on acrylic boards in different scenarios (wearing socks, flat insoles, medical insoles) and measure plantar pressure through thin film pressure sensors placed in each area. Table II shows the mean pressure in static plantar experiments.

TABLE II. MEAN PRESSURE IN STATIC PLANTAR EXPERIMENTS

Experimental method	1	2	3	4	5	6	7	8
Wearing socks	12.9	39.3	37.5	32.6	0.9	16.2	48.1	42.5
Ordinary insoles	5.4	34.4	24.5	27.3	0.9	11.8	34.5	36.2
Intelligent insoles	6.5	31.3	14.9	16.8	19.3	19.9	35.2	29.7

In Table II, labels 1-8 represent the first metatarsal region, the first metatarsal region, the second and third metatarsal regions, the fourth and fifth metatarsal regions, the lateral midfoot region, the arch region, the medial heel region, and the lateral heel region, respectively. Compared to the control group wearing socks and the regular insole, wearing smart insoles effectively reduces plantar pressure. The intelligent insole specifically optimizes the pressure distribution in the second and third metatarsal regions, fourth and fifth metatarsal regions, and the lateral side of the heel, while increasing pressure in the arch and medial areas of the foot. This indicates that the ASS and multi stiffness characteristics of intelligent insoles have to some extent reduced plantar pressure, but the pressure relief effect on the inner side of the sole can still be further improved.

B. Application Analysis of GR Algorithm

Fifteen subjects are selected for gait data collection in the experiment to form a dataset consisting of different time series lengths. The experiment divides the dataset into training, validation, and testing sets in a 6:2:2 ratio. The experiment uses ConvBiGru-FCN to train the data and achieve recognition of different gaits. To verify the effectiveness of ConvBiGru-FCN, Multi-layer Perceptron (MLP), Time-CNN, and FCN are used as contrast networks in the experiment. The convolution kernel size of ConvBiGru-FCN convolutional layer is 3 × 3, with a step size of 1. The hidden state size of the BiGru layer is 128, and in the fully convolutional layer, the number of output channels is the corresponding number of categories. The number of neurons in the fully connected layer between the MLP input layer and output layer is 128. The ReLU activation function is used, and the Softmax function is used for multi classification in the output layer. The convolutional kernel size of the Time CNN convolutional layer is 3×3 with a step size of 1, and the pooling kernel size of the pooling layer is 2×2 with a step size of 2. The experiment set the time series length to 60, and the performance comparison results of different networks are shown in Fig. 11.

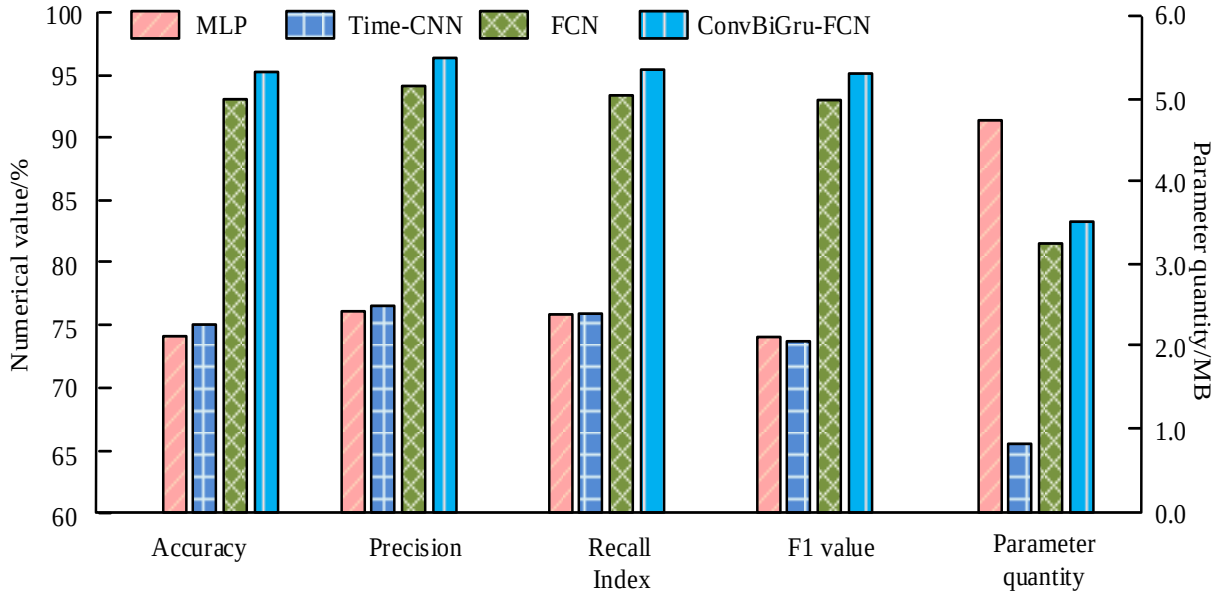

Fig. 11. Performance comparison results of different networks.

In Fig. 11, there are significant differences in the performance of various models in identifying subject identities when the sequence length is 60. ConvBiGru-FCN outperforms other networks in terms of accuracy, precision, recall, and F1 score. The accuracy of ConvBiGru-FCN reaches 95.26%, which is 2.03% higher than FCN, while its parameter count is only 3.42M, slightly higher than FCN. This indicates that ConvBiGru-FCN is an effective feature extraction method and exhibits good performance in GR tasks. The visualization results of network feature extraction are shown in Fig. 12.

In Fig. 12, the numbers 1-15 represent the features of 15 users, respectively. Fig. 12(a) to (d) show the visualization results of feature extraction for MLP, Time-CNN, FCN, and ConvBiGru-FCN networks, respectively. ConvBiGru-FCN has a good discriminative effect in identifying different gait identity categories. In contrast, MLP, Time-CNN, and FCN have poorer performance in distinguishing identity categories. This indicates that ConvBiGru-FCN has a high feature extraction ability in GR tasks and can effectively extract gait information from subjects. The relative error of ConvBiGru-FCN gait prediction in both stationary and walking states of the human body is Fig. 13.

In Fig. 13, under both stationary and walking states, the calculated curve of user GR in ConvBiGru-FCN is generally close to the true value, and the relative error of user GR prediction is mostly in the range of 0% -8%, indicating a good overall fitting effect. To verify the effectiveness of the proposed GR algorithm combined with BPRSWDs, the pressure curve is used as the validation object for the GR algorithm in the experiment. The variation curves of proportional signal and fuzzy output signal are shown in Fig. 14.

Fig. 14 (a) (b) shows the variation curves of the proportional signal and the fuzzy output signal. The fuzzy output signals u_1, u_2, and u_3 are used to divide the early and middle stages of the support phase, the middle and late stages of the support phase, and the support phase and swing phase, respectively. There is a difference in the proportion of left and right feet in each stage of the gait cycle. The initial proportion of support for the left foot is too long, which may be related to the high support structure of the left foot insole, resulting in a prolonged force on the heel and a reduced contact time between the forefoot and the ground. The proportion of SSP and double support phases during walking is obtained by combining the fuzzy output signals of the left and right feet, which are 92.7% and 7.3%, respectively.

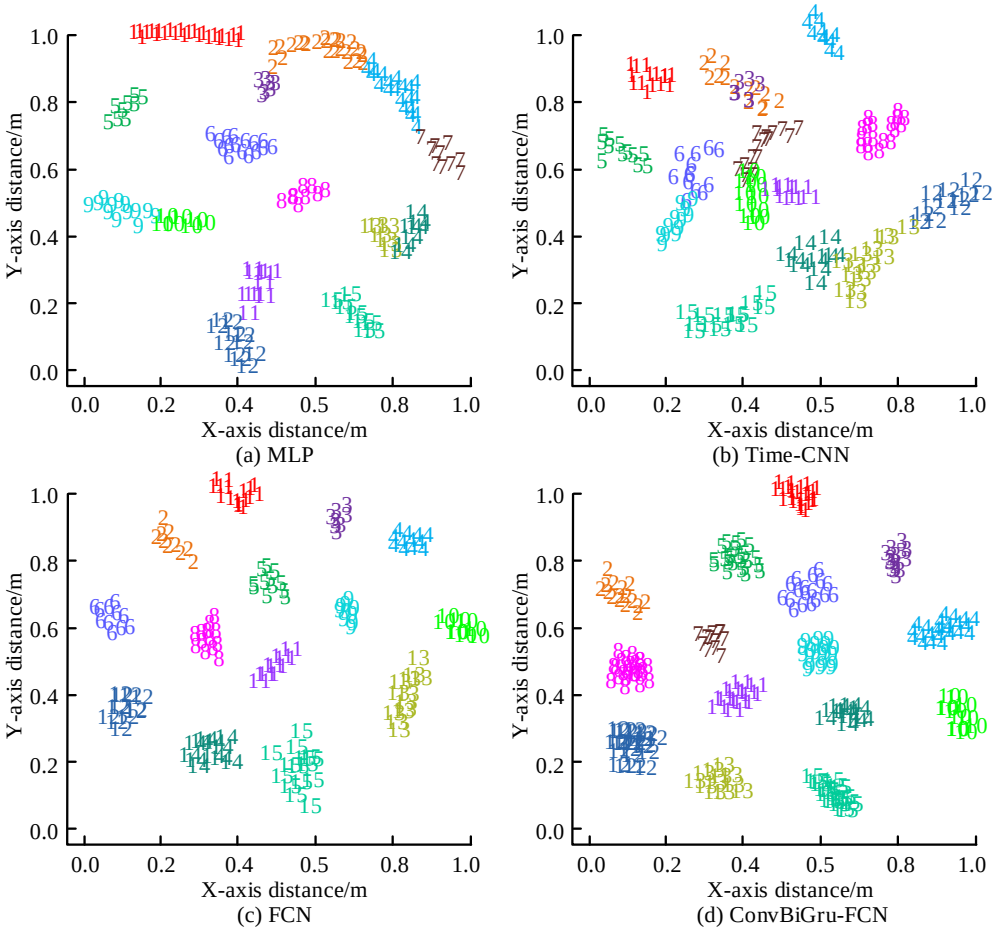

Fig. 12. Visualization of network feature extraction results.

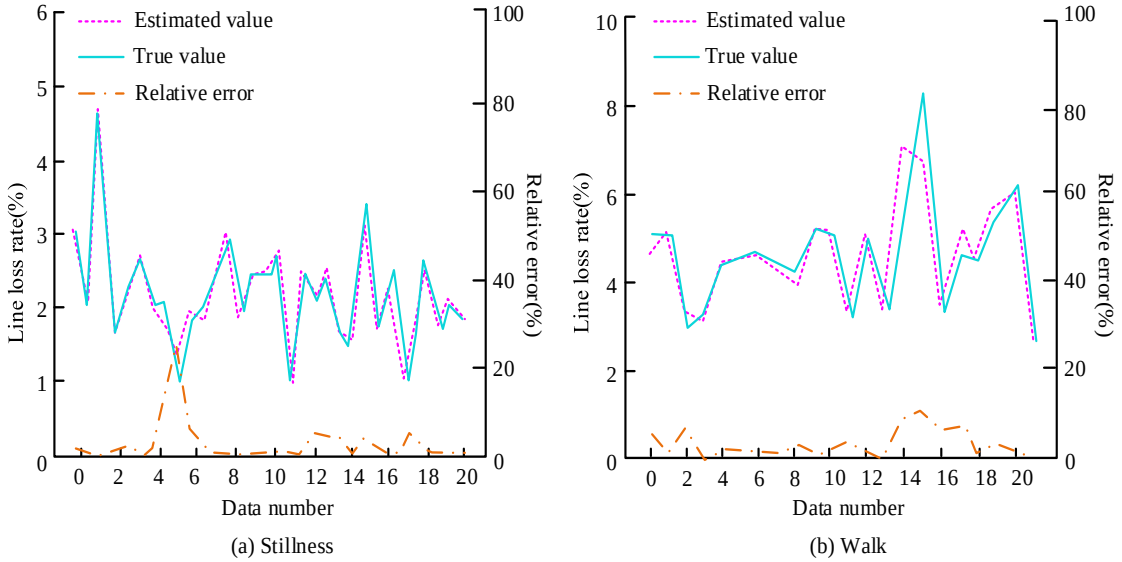

Fig. 13. Relative error of user gait recognition.

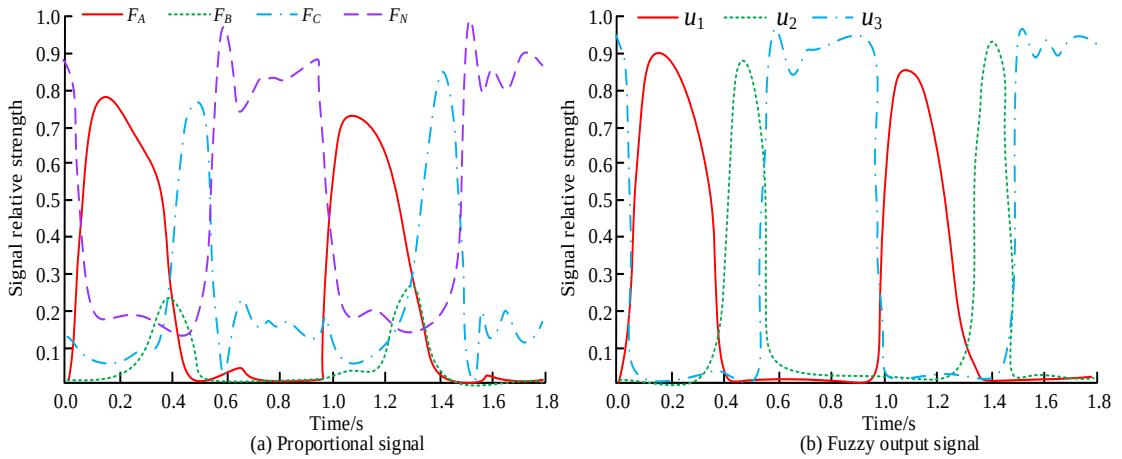

Fig. 14. Visualization of network feature extraction results.

C. Discussion

Research has been conducted to manufacture intelligent insoles with pressure reduction effects through 3D printing technology, and the pressure reduction effect of intelligent insoles has been verified by comparing the EMGS of natural walking and walking with exoskeletons. When training the GR algorithm, ConvBiGru-FCN was studied and compared with other networks. In the process of manufacturing and forming BPRSWDs, the 3D printing parameters were optimized experimentally, and the pressure distribution of the feet was measured using the Flexiforce A201 thin pressure sensor. The experimental results show that compared to the natural state, when walking with smart insoles, the pressure distribution of the feet is effectively optimized, especially in the second and third metatarsal regions, fourth and fifth metatarsal regions, as well as the pressure distribution in the arch and medial heel regions. ConvBiGru-FCN has high accuracy, precision, recall, and F1 score in identifying different walking postures, with an accuracy rate of 95.26%. In addition, we also visualized the network feature extraction, and the results showed that ConvBiGru-FCN has good discriminative performance and can effectively extract walking information from subjects. When standing and walking, the calculated curve of ConvBiGru-FCN is approximately close to the true value, with a relative error between 0% and 8%, indicating a good overall fitting effect. This study provides a new method for the design and manufacturing of intelligent insoles. By combining the GR algorithm, it can achieve recognition of walking posture and optimization of pressure distribution, thereby improving walking comfort and reducing foot pressure.

V. Conclusion

This study optimized BPRSWDs, including insoles and ankle exoskeletons, through 3D-PT design, and combined them with the GR algorithm to achieve individual identity recognition and gait analysis. This study used a dual track treadmill platform and evaluated the decompression support effect of ankle exoskeletons through comparative experiments with EMGS. Meanwhile, the pressure reducing effect of the intelligent insole was verified through static plantar pressure

experiments. The results showed that compared to the natural state, the EMGS integral values of the gastrocnemius and tibialis anterior muscles decreased by 5.4% and 3.6% respectively when walking with exoskeletons. This indicated that the contraction characteristics of the lower limb muscles had been weakened, and the ankle exoskeleton had a certain assisting effect. In addition, the ASS and multi stiffness characteristics of smart insoles to some extent reduced plantar pressure. In terms of GR algorithm, the accuracy of ConvBiGru-FCN reached 95.26%, which was 2.03% higher than FCN. Moreover, the study also processed the plantar pressure signal through fuzzy logic, achieving an analysis of the proportion of SSP and double support phases during walking. In summary, this study achieved the optimization design of BPRSWDs through the fusion of 3D-PT and GR algorithms, providing useful references for research in the fields of GR and body decompression support. However, there are still some limitations to this study, such as a small sample size and the need to improve the generalization ability of the GR algorithm. Future research can further expand the sample size, enhance the generalization ability of the GR algorithm, and explore more optimization design solutions to achieve more precise and intelligent design of BPRSWDs.

ACKNOWLEDGMENT

The research is supported by: The Philosophy and Social Science Planning Project of Anhui Province in 2020, (NO. AHSKY2020D110).

REFERENCES

[1] Y. Zhu, F. Sun, C. Jia, C. Huang, K. Wang, Y. Li, L. Chou and Y. Mao. "A 3D printing triboelectric sensor for gait analysis and virtual control based on human-computer interaction and the internet of things," Sustainability., vol. 14, no. 17, pp. 10875-10886, August, 2022, DOI: 10.3390/su141710875.

[2] Q. Zhang, T. Jin, J. Cai, L. Xu, T. He, Y. Tian, L. Li, Y. Peng and C. Lee. "Wearable triboelectric sensors enabled gait analysis and waist motion capture for IoT-based smart healthcare applications," Adv. Sci., vol. 9, no. 4, pp. 2103694-2103706, November, 2022, DOI: 10.1002/advs.202103694.

[3] M. Bhatnagar, S. Jha and A. Pattnaik A. "Analysis of different printing technologies for metallization of crystalline silicon solar cells," Int. J. Mater. Res., vol. 114, no. 7, pp. 518-526, March, 2023, DOI: 10.1515/ijmr-2021-8686.

[4] N. Li and X. Zhao. "A multi-modal dataset for gait recognition under occlusion," Appl. Intell., vol. 53, no. 2, pp. 1517-1534, January, 2023, DOI: 10.1007/s10489-022-03474-8.

[5] C. Meng, X. He and T. L. Luan. "Gait recognition based on 3D human body reconstruction and multi-granular feature fusion," J. Supercomput., vol. 79, no. 11, pp. 12106-12125, July, 2023, DOI: 10.1007/s11227-023-05143-0.

[6] A. Peki and E. Bülent E. "Experimental and statistical analysis of robotic 3D printing process parameters for continuous fiber reinforced composites," J. Compos. Mater., vol. 55, no. 19, pp. 2645-2655, February, 2021, DOI: 10.1177/0021998321996425.

[7] Z. Yu, X. Yang, G. Wei, L. Wang, K. Wang, W. Chen and J. Wei. "A Novel High-Current Planar Inductor with Cooling Fins Based on 3D Printing," IEEE T. Power Electr., vol. 36 no. 11, pp. 12189-12195, May, 2021, DOI: 10.1109/TPEL.2021.3078083.

[8] Z. Wu, Y. Jin, G. Li, M. Zhang and J. Du. "Strain Sensing Behavior of 3D Printable and Wearable Conductive Polymer Composites Filled with Silane-Modified MWCNTs," Macromol. Rapid Comm., vol. 43 no. 4, pp. 2100663-2100672, February, 2021, DOI: 1002/marc.202100663.

[9] S. Zhang, Y. Liu, J. Hao, G. Wallace, S. Beirne and J. Chen. "3D-printed Wearable Electrochemical Energy Device," Adv. Funct. Mater., vol. 32 no. 3, pp. 2103092-2103124, July, 2021, DOI: 10.1002/adfm.202103092.

[10] H. Liu, H. Zhang, W. Han, H. Lin, R. Li, J. Zhu and W. Huang. "3D Printed Flexible Strain Sensors: From Printing to Devices and Signals," Adv. Mater., vol. 33 no. 8, pp. 2004782-2004800, January, 2021, DOI: 10.1002/adma.202004782.

[11] W. Hong, X. Guo and T. Zhang T. "Flexible Capacitive Pressure Sensor with High Sensitivity and Wide Range Based on a Cheetah Leg Structure via 3D Printing," ACS Appl. Mater. Inter., vol. 15 no. 39, pp. 46347-46356, September, 2023, DOI: 10.1021/acsami.3c09841.

[12] S. Bianco, P. Napoletano, A. Raimondi and M. Rima. "U-WeAr: User Recognition on Wearable Devices through Arm Gesture," IEEE T. Hum-mach. Syst., vol. 52, no. 4, pp. 713-724, August, 2022. DOI: 10.1109/THMS.2022.3170829.

[13] Y. J. Lee, M. Y. Wei and Y. J. Chen Y J "Multiple inertial measurement unit combination and location for recognizing general, fatigue, and simulated-fatigue gait," Gait Posture., vol. 96, no. 1, pp. 330-337, July, 2022. DOI: 10.1016/j.gaitpost.2022.06.011.

[14] V. B. Semwal, A. Gupta A and P. Lalwani. "An optimized hybrid deep learning model using ensemble learning approach for human walking activities recognition," J. Supercomput., vol. 77, no. 11, pp. 12256-12279, November, 2021. DOI: 10.1007/s11227-021-03768-7.

[15] D. Ma, G. Lan, W. Xu, M. Hassan and W. Hu. "Simultaneous Energy Harvesting and Gait Recognition Using Piezoelectric Energy Harvester," IEEE T. Mobile Comput., vol. 21, no. 6, pp. 2198-2209, June, 2022. DOI: 10.1109/TMC.2020.3035045.

[16] M. M. Hasan and H. A. Mustafa. "Learning view-invariant features using stacked autoencoder for skeleton-based gait recognition," IET Comput. Vis., vol. 15, no. 7, pp. 527-545, April, 2021. DOI: 10.1049/cvi2.12050.

[17] C. Zhang, Q. Chen, M. Wang and S. Wei. "Optimised two-dimensional orthogonal matching pursuit algorithm via singular value decomposition," IET Signal Process., vol. 14, no. 4, pp. 717-724, December, 2021, DOI: 10.1049/iet-spr.2019.0090.

[18] A. Sezavar, R. Atta and M. Ghanbari M. "Smartphone-based gait recognition using convolutional neural networks and dual-tree complex wavelet transform," Multimedia Syste., vol. 28, no. 6, pp. 2307-2317, June, 2022, DOI: 10.1007/s00530-022-00954-2.

[19] I. Rojek, J. Dorożyński, D. Mikołajewski and P. Kotlarz. "Overview of 3D printed exoskeleton materials and opportunities for their AI-based optimization," Appl. Sci., vol. 13, no. 14, pp. 8384-8399, June, 2023, DOI: 10.3390/app13148384.

[20] A. G. Samarentsis, G. Makris, S. Spinthaki, G. Christodoulakis, M. Tsiknakis and A. K. Pantazis. "A 3D-Printed Capacitive Smart Insole for Plantar Pressure Monitoring," Sensors., vol. 22, no. 24, pp. 9725-9742, December, 2022, DOI: 10.3390/s22249725.

[21] C. Zhang, Z. Feng, Z. Gao, X. Jin, D. Yan and L. Yi. "Salient feature multimodal image fusion with a joint sparse model and multiscale dictionary learning," Opt. Eng., vol. 59, no. 5, pp. 51402-51420, December, 2019, DOI: 10.1117/1.OE.59.5.051402.

[22] L. Zhou and T. Jiang. "Learning body part-based pose lexicons for semantic action recognition," IET Comput. Vis., vol. 17, no. 2, pp. 135-155, September, 2023, DOI: 10.1049/cvi2.12143.

[23] J. Wu, J. Wang, Q. Gao, M. Pan and H. Zhang. "Path-Independent Device-Free Gait Recognition Using mmWave Signals," IEEE T. Veh. Technol., vol. 70, no. 11, pp. 11582-11592, November, 2021, DOI: 10.1109/TVT.2021.3111600.

[24] A. Filatov, and K. Krinkin. "A Simplistic Approach for Lightweight Multi-Agent SLAM Algorithm," Inter. Jour. Embed. Real-Tim., vol. 11, no. 3, pp. 67-83, July, 2020, DOI: 10.4018/IJERTCS.2020070104.

[25] S. Gao, J. Yun, Y. Zhao and L. Liu. "Gait-D: Skeleton-based gait feature decomposition for gait recognition," IET Comput. Vis., vol. 16, no. 2, pp. 111-125, November, 2022, DOI: 10.1049/cvi2.12070.

[26] Y. Zhong and Q. Yan. "Spatio-temporal stacking model for skeleton-based action recognition," Appl. Intell., vol. 52, no. 11, pp. 12116-12130, September, 2022, DOI: 10.1007/s10489-021-02994-z.

[27] L. Xu, H. Yin, T. Shi, D. Jiang, and B. Huang. "EPLF-VINS: Real-Time Monocular Visual-Inertial SLAM with Efficient Point-Line Flow

Features," IEEE Robot. Autom. Let., vol. 8, no. 2, pp. 752-759, December, 2022, DOI: 10.1109/LRA.2022.3231983.

[28] X. Tan , B. Zhang , G. Liu , X. Zhao and Y. Zhao. "Phase Variable Based Recognition of Human Locomotor Activities Across Diverse Gait Patterns," IEEE T. Hum-Mach. Syst., vol. 51, no. 6, pp. 684-695, December, 2021, DOI: 10.1109/THMS.2021.3107256.

[29] J. Wu. "A fast-iterative reconstruction algorithm for sparse angle CT based on compressed sensing," Future Gener. Comp. Sy., vol. 126, no. 1, pp. 289-294, August, 2022, DOI: 10.1016/j.future.2021.08.013.

[30] N. Luo, H. Yu, Z. You, Y. Li, T. Zhou, N.s Han, C. Liu, Z. Jiang and S. Qiao. "Fuzzy logic and neural network-based risk assessment model for import and export enterprises: A review," J. Data Sci. Intell. Syst., vol. 1, no. 1, pp. 2-11, June, 2023, DOI: 10.47852/bonviewJDSIS32021078.

[31] A. M. Usman and M. K. "Abdullah An Assessment of Building Energy Consumption Characteristics Using Analytical Energy and Carbon Footprint Assessment Model," Green and Low-Carbon Econ., vol. 1, no. 1, pp. 28-40, February, 2023, DOI:10.47852/bonviewGLCE3202545.